

Lattice-Entangled Density Wave Instability and Nonthermal Melting in $\text{La}_4\text{Ni}_3\text{O}_{10}$

Chen Zhang,^{1,*} Lixing Chen,^{2,3,*} Qi-Yi Wu,¹ Congcong Le,⁴ Xianxin Wu,⁵ Hao Liu,¹ Bo Chen,¹ Ying Zhou,¹ Zhong-Tuo Fu,¹ Chun-Hui Lv,¹ Zi-Jie Xu,¹ Hai-Long Deng,¹ Enkang Zhang,^{2,3} Yinghao Zhu,^{2,3} H. Y. Liu,⁶ Yu-Xia Duan,¹ Jun Zhao,^{2,3,†} and Jian-Qiao Meng^{1,‡}

¹School of Physics, Central South University, Changsha 410012, Hunan, China

²State Key Laboratory of Surface Physics and Department of Physics, Fudan University, Shanghai, China

³Shanghai Research Center for Quantum Sciences, Shanghai, China

⁴Hefei National Laboratory, and New Cornerstone Science Laboratory, Hefei, Anhui 230088, China

⁵Institute of Theoretical Physics, Chinese Academy of Sciences, Beijing 100190, China

⁶Beijing Academy of Quantum Information Sciences, Beijing 100085, China

(Dated: Tuesday 30th December, 2025)

The recent discovery of high-temperature superconductivity in pressurized nickelates has renewed interest in the broken-symmetry states of their ambient-pressure parent phases, where a density-wave (DW) order emerges and competes with superconductivity, but its microscopic origin remains unresolved. Using ultrafast optical spectroscopy, we track quasiparticle relaxation dynamics across the DW transition at $T_{\text{DW}} \approx 136$ K in trilayer nickelate $\text{La}_4\text{Ni}_3\text{O}_{10}$ single crystals, revealing the opening of an energy gap of ~ 52 meV. Multiple coherent phonons, including A_g modes near 3.88, 5.28, and 2.09 THz, display pronounced mode-selective anomalies across the transition, demonstrating that the DW is coupled with lattice degree of freedom stabilized through electron-phonon coupling. At higher excitation densities, the DW is nonthermally suppressed, producing a temperature-fluence phase diagram that parallels pressure-tuned behavior. These results establish the DW in $\text{La}_4\text{Ni}_3\text{O}_{10}$ as a lattice-entangled instability involving multiple phonon modes, and highlight ultrafast optical excitation as a powerful tool to manipulate competing orders in nickelates.

The interplay between superconductivity (SC) and density-wave (DW) order is a defining yet unresolved theme in correlated electron systems. In the Ruddlesden-Popper nickelates $\text{La}_{n+1}\text{Ni}_n\text{O}_{3n+1}$, superconductivity emerges when a native DW order is suppressed under hydrostatic pressure, suggesting that the DW quantum critical point plays a central role in their phase diagram [1–8]. This competition mirrors the cuprates and iron pnictides, where charge and spin orders are closely entwined with superconductivity [9, 10]. Notably, tetragonal $\text{La}_4\text{Ni}_3\text{O}_{10}$ fails to superconduct even under pressures up to 160 GPa in the absence of a DW instability [11], underscoring the intimate link between superconductivity and density-wave physics.

The bilayer $\text{La}_3\text{Ni}_2\text{O}_7$ has been the focus of extensive study, yet sample quality limitations have led to conflicting reports on its DW properties [12–16]. In contrast, the trilayer $\text{La}_4\text{Ni}_3\text{O}_{10}$ displays high crystalline quality and undergoes a robust spin-charge density-wave transition at $T_{\text{DW}} \approx 136$ K [2, 17], making it an ideal platform for investigating the ordered state. The central ambiguity, however, is the DW's microscopic origin, with conflicting evidence pointing to either single d_{z^2} or hybridized $d_{x^2-y^2}/d_{z^2}$ orbital physics [18–27]. Clarifying this orbital character is crucial for understanding the mechanism of DW formation. Resolving this requires a probe sensitive to both the electronic gap dynamics and the associated lattice symmetry breaking.

Ultrafast optical spectroscopy provides a uniquely powerful means to address this issue. Its femtosecond resolution allows direct observation of quasiparticle relaxation across an energy gap, while coherent lattice vibrations launched by photoexcitation reveal phonon modes that couple to symmetry breaking [28–30]. By monitoring the temperature evolution of both quasiparticle and phonon responses, ultrafast spectroscopy exposes the cooperative dynamics of electronic cor-

relations and lattice distortions that stabilize the density-wave phase—capabilities not easily achieved by static probes such as ARPES or Raman scattering.

Here we use ultrafast optical spectroscopy to probe $\text{La}_4\text{Ni}_3\text{O}_{10}$. We report three main findings: (i) quasiparticle relaxation dynamics reveal the opening of a strong-coupling 52 meV DW gap at T_{DW} ; (ii) a phonon at 3.88 THz undergoes anomalous renormalization directly linked to the DW order

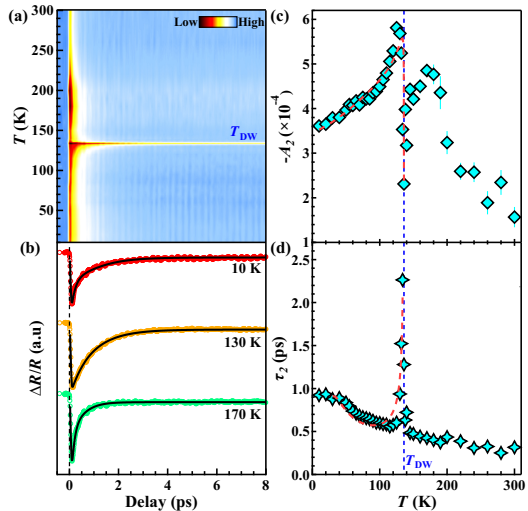


FIG. 1. **Quasiparticle dynamics across the DW transition.** (a) Transient reflectivity $\Delta R(t)/R$ as a function of temperature and time delay, measured at a low pump fluence of $\sim 10.2 \mu\text{J}/\text{cm}^2$. The sharp change at T_{DW} marks the phase transition. (b) Representative $\Delta R(t)/R$ traces at different temperatures. Black lines are fits using a bi-exponential model. (c, d) Temperature dependence of the amplitude (A_2) and lifetime (τ_2) of the slow relaxation component. Dashed red curves are fits to the RT model.

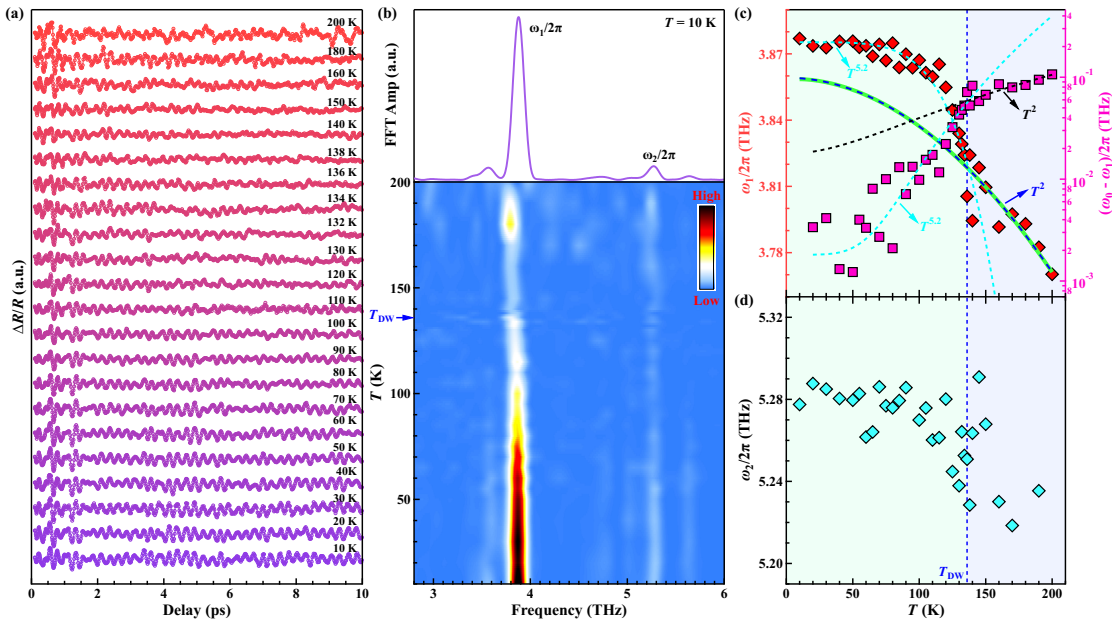


FIG. 2. **Anomalous phonon dynamics at low pump fluence.** (a) Coherent oscillations at select temperatures, isolated by subtracting the quasiparticle background. Traces are offset for clarity. (b) Corresponding FFT map, showing the temperature evolution of the two most prominent phonon modes, ω_1 and ω_2 . (c) Temperature dependence of the ω_1 mode frequency. The solid green line is a fit to a standard anharmonic decay model, which the data clearly deviates from below T_{DW} . Dashed curves are power-law fits (T^2 above T_{DW} , $T^{5.2}$ below), and the right axis shows the data on a log-log scale to highlight the change in slope at the transition. (d) Temperature dependence of the ω_2 mode frequency.

parameter, signaling strong e - ph coupling and multi-orbital involvement; and (iii) intense optical excitation suppresses the DW nonthermally, yielding a temperature-fluence phase diagram analogous to pressure tuning. Together, these results provide new insight into the microscopic nature of the DW in $\text{La}_4\text{Ni}_3\text{O}_{10}$ and demonstrate light as an effective control knob for competing orders in nickelates.

High-quality single crystals of $\text{La}_4\text{Ni}_3\text{O}_{10}$ were grown using a high-pressure optical floating-zone furnace (HKZ, SciDre GmbH; 5 kW xenon lamp) under 18 to 22 bar O_2 [2]. Transient differential reflectivity $\Delta R(t)/R$ was measured using a pump-probe setup with an Yb-based femtosecond oscillator operating at 1 MHz and a central wavelength of 800 nm (1.55 eV) [31]. To improve the signal-to-noise ratio, the pump and probe beams are linearly orthogonally polarized, and a polarizer is placed in front of the detector to filter out the scattered pump beam. Temperature-dependent weak-fluence measurements were performed on sample S1, while other measurements used sample S2 from the same batch.

Figure 1(a) maps the transient reflectivity $\Delta R(t)/R$ across the DW transition at a low pump fluence of $\sim 10.2 \mu\text{J}/\text{cm}^2$. Each trace [Fig. 1(b)] consists of a non-oscillatory quasiparticle (QP) relaxation alongside coherent oscillations. The QP dynamics are well described by a bi-exponential decay (see Sec. I of the Supplemental Material [32]), consisting of a fast component (τ_1) from carrier thermalization via electron-electron (e - e) and (e - ph) scattering, and a slower component (τ_2) associated with recombination across the DW gap. The latter provides a direct probe of the ordered state.

As shown in Figs. 1(c) and 1(d), the amplitude A_2 and life-

time τ_2 exhibit sharp anomalies at $T_{DW} \approx 136$ K. Most notably, τ_2 diverges, revealing critical slowing down characteristic of a second-order phase transition. This dynamic signature confirms the opening of an energy gap [28, 29]. By fitting with the Rothwarf-Taylor (RT) model [33, 34], which accounts for phonon bottleneck recombination, we extract a zero-temperature gap of $2\Delta_{DW}(0) \approx 52$ meV (see Sec. II of the Supplemental Material [32]), consistent with some other spectroscopic studies [24, 25]. The ratio $2\Delta_{DW}(0)/k_B T_{DW} \approx 4.4$ exceeds the weak-coupling BCS value, identifying $\text{La}_4\text{Ni}_3\text{O}_{10}$ as a strong-coupling system. This ratio, however, is substantially smaller than that found in bilayer $\text{La}_3\text{Ni}_2\text{O}_7$ (~ 11) [37], pointing to fundamental differences between trilayer and bilayer nickelates in how density-wave order is stabilized.

Having characterized the electronic gap, we now analyze the coherent lattice oscillations to examine e - ph coupling. Figure 2(a) presents the time-domain traces after subtracting the QP background, while Fig. 2(b) shows the corresponding fast Fourier transform (FFT) spectra. Two prominent A_g symmetry phonons are resolved (see Sec. III of the Supplemental Material [32]): $\omega_1 \approx 3.88$ THz (129.4 cm^{-1}) and $\omega_2 \approx 5.28$ THz (176.1 cm^{-1}) at 10 K, in agreement with Raman measurements [19, 20]. Both modes soften with increasing temperature, but ω_1 exhibits a pronounced anomaly at T_{DW} . Above the transition, ω_1 follows standard anharmonic phonon decay [38, 39]. Below T_{DW} , however, it deviates sharply, showing a much stronger temperature dependence [see Fig. 2(c)]. A power-law analysis ($\omega_1(T) = \omega_1(0) - \alpha T^n$) quantifies this change [40]: the exponent n switches from $n = 2$ (anharmonic theory) above T_{DW} to $n \approx 5.2$ below it, which

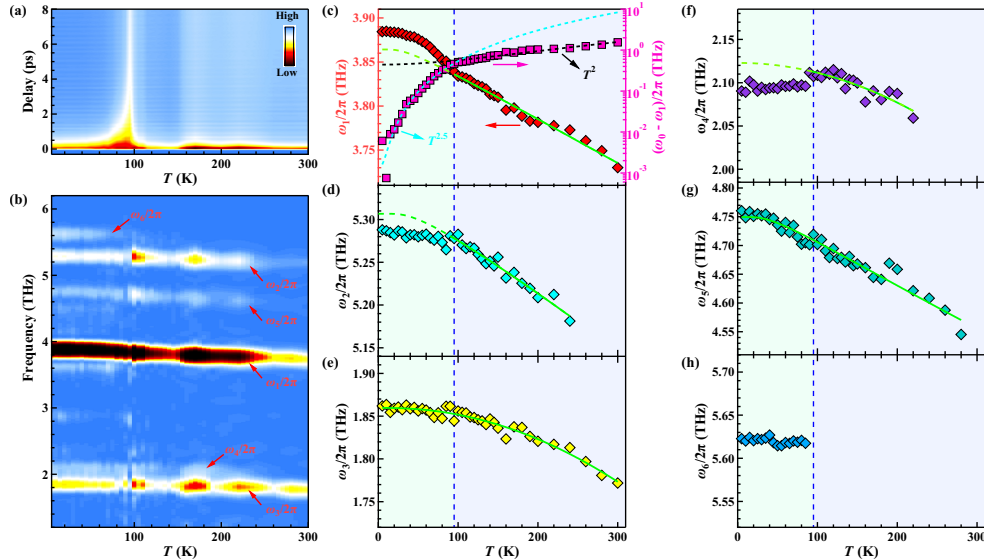


FIG. 3. **Full phonon spectrum and mode-selective coupling at high pump fluence.** (a) raw $\Delta R(t)/R$ map measured at a high pump fluence of $\sim 130 \mu\text{J}/\text{cm}^2$, which suppresses the transition to $T_{\text{DW}} \approx 95 \text{ K}$. (b) Corresponding FFT map revealing six distinct coherent phonon modes (ω_1 to ω_6). (c-h) Temperature dependence of the frequency for each of the six modes. Vertical dashed lines indicate the suppressed T_{DW} . Solid green lines are fits to the anharmonic decay model, highlighting the anomalous behavior of modes ω_1 and ω_4 below the transition.

is highlighted in the log-log plot shown on the right axis of Fig. 2(c). This abrupt change signals a new phonon decay channel coupled directly to the DW order parameter. This abrupt renormalization demonstrates strong coupling between ω_1 and the density-wave instability.

To uncover weaker lattice modes, we increased the pump fluence to $130 \mu\text{J}/\text{cm}^2$ (Fig. 3). Under these conditions, the transition temperature is suppressed to $T_{\text{DW}} \approx 95 \text{ K}$ [Fig. 3(a)]. Remarkably, despite this $\sim 30\%$ reduction in T_{DW} , the ground-state gap remains nearly unchanged at $2\Delta_{\text{DW}}(0) \approx 55 \text{ meV}$ (see Sec. II of the Supplemental Material [32]). This behavior yields an enhanced coupling ratio $2\Delta_{\text{DW}}(0)/k_B T_{\text{DW}} \approx 6.6$, compared to ~ 4.4 at low fluence. The robustness of the gap in the face of reduced T_{DW} highlights a strikingly nonthermal effect of photoexcitation: instead of simply suppressing order, light drives $\text{La}_4\text{Ni}_3\text{O}_{10}$ deeper into a strong-coupling regime. This contrasts sharply with hydrostatic pressure, where both T_{DW} and the gap are monotonically reduced [25], and with bilayer $\text{La}_3\text{Ni}_2\text{O}_7$, where the gap diminishes under increasing fluence, leading to a reduced ratio [37]. Thus, the density wave in $\text{La}_4\text{Ni}_3\text{O}_{10}$ is unusually robust against photodoping, reflecting a lattice-stabilized mechanism.

At high fluence, four additional phonon ($\omega_3 - \omega_6$) resolved [Fig. 3(b)] (see Sec. III of the Supplemental Material [32]), revealing a richer picture of mode-selective coupling [Figs. 3(c)-3(h)]. The ω_1 mode retains its anomalous renormalization at the reduced T_{DW} , transitioning from T^2 behavior above the transition to $T^{2.5}$ scaling within the ordered phase [Fig. 3(c)]. While the precise exponent depends somewhat on excitation density, the robust crossover at T_{DW} and the consistent T^2 scaling above it confirm that ω_1 is intrinsically tied to the density-wave order. Its eigenvector involves apical oxygen motion, Ni-O plane bending, and La displacements [20, 27],

signifying a multi-component lattice vibration. Such complexity rules out a single-orbital instability and instead supports a multi-orbital mechanism, consistent with ARPES evidence linking the DW gap to interorbital hybridization [22].

Importantly, the ω_2 phonon [Fig. 3(d)] also exhibits anomalous renormalization, but in the opposite direction: instead of hardening like ω_1 , ω_2 softens below T_{DW} . The contrasting behavior of these two A_g modes underscores that the density-wave order couples to multiple phonons in distinct ways, highlighting the complex, mode-dependent nature of $e\text{-}ph$ interactions in $\text{La}_4\text{Ni}_3\text{O}_{10}$.

Another key anomaly appears in the ω_4 mode ($\approx 2.09 \text{ THz}$) [Fig. 3(f)], which softens significantly below T_{DW} . This behavior is strongly reminiscent of phonon renormalization at the charge-density-wave onset in cuprate superconductors [41–43], where gap opening modifies $e\text{-}ph$ coupling and drives anomalous phonon softening [42]. This analogy suggests that lattice anomalies in nickelates and cuprates may share a common origin in charge ordering. Such behavior reinforces the intimate connection between charge order and superconductivity in layered correlated systems. By contrast, the ω_3 ($\approx 1.86 \text{ THz}$) and ω_5 ($\approx 4.76 \text{ THz}$) modes [Figs. 3(e) and 3(g)] follow ordinary anharmonic decay, serving as internal controls that confirm the selectivity of the anomalous coupling.

Finally, the ω_6 mode ($\approx 5.62 \text{ THz}$) appears only below T_{DW} [Fig. 3(h)]. Its sudden onset rules out a conventional amplitude mode and suggests alternative origins, such as reduced metallic screening due to partial Fermi-surface gapping [20] or zone-folding from symmetry lowering [44]. Its weak intensity in our data prevents a conclusive assignment, motivating further experiments.

Beyond serving as a probe, the pump laser also acts as a

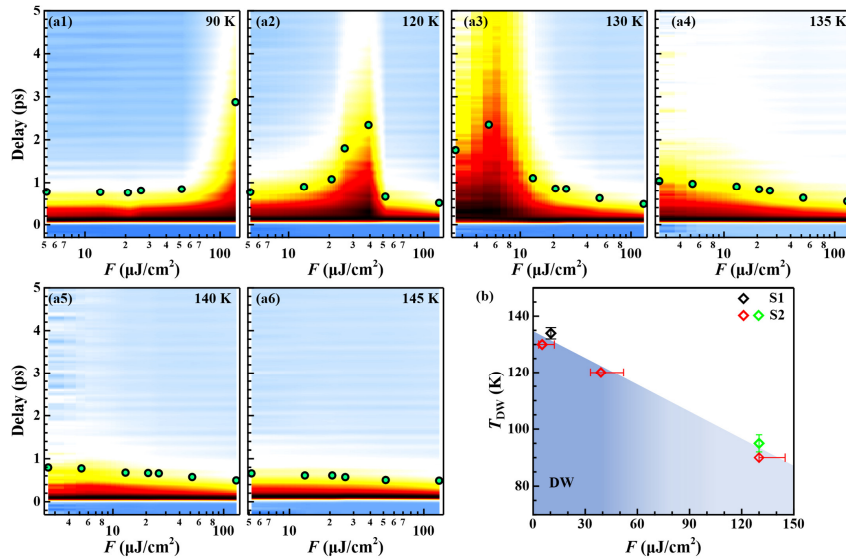


FIG. 4. **Non-thermal melting of the DW order.** (a1)-(a6) Normalized $\Delta R(t)/R$ maps as a function of pump fluence at several fixed temperatures. The black circles trace the slow relaxation time τ_2 , which peaks at the critical fluence F_C required to melt the DW order. (b) The resulting Temperature-Fluence phase diagram for $\text{La}_4\text{Ni}_3\text{O}_{10}$. The phase boundary is determined by the $F_C(T)$ values, extracted from the peaks in τ_2 shown in panel (a), together with data from Figs. 1 (black symbol) and 3 (green symbol).

tuning parameter for the ordered phase [29, 45, 46]. Figures 4(a1)-4(a6) show how the QP relaxation evolves with fluence at fixed temperatures. Below T_{DW} , the slow component τ_2 increases with fluence, peaks at a critical fluence F_C , and then collapses, signaling complete melting of the density-wave condensate. The resulting temperature-fluence phase diagram [Fig. 4(b)] shows that F_C grows as the system is cooled, increasing from $\sim 5.2 \mu\text{J}/\text{cm}^2$ at 130 K to over $130 \mu\text{J}/\text{cm}^2$ at 90 K. This behavior resembles pressure-tuned suppression of the DW [25, 47], but with a crucial difference: under pressure, both T_{DW} and the gap decrease together [25, 47], while in $\text{La}_3\text{Ni}_2\text{O}_7$ optical excitation suppresses them simultaneously [37]. In $\text{La}_4\text{Ni}_3\text{O}_{10}$, however, light reduces T_{DW} while preserving the gap, yielding an enhanced ratio. Even at the highest fluence, the steady-state temperature rise is estimated at only ~ 8 K (see Sec. IV of Supplemental Material [32]), far smaller than the observed ~ 40 K suppression of T_{DW} . Thus, optical excitation reshapes the free-energy landscape directly, providing a distinctly nonequilibrium pathway to control competing orders in nickelates.

Experimental data indicate an intrinsic coupling between the DW order and lattice degrees of freedom in trilayer nickelates. The DW state comprises intertwined SDW and CDW: the SDW component is dominantly localized on the outer NiO_2 layers, whereas the CDW modulates all three layers [17]. The key difference between the ω_1 and ω_2 phonon modes lies in the distinct motion of the inner-layer oxygen atoms [32]. Consequently, the distinct temperature dependences of ω_1 and ω_2 phonon frequencies below T_{DW} point to a selective coupling of the lattice to the CDW component of the DW state. This interpretation is consistent with the observed isotope dependence of T_{DW} in $\text{La}_4\text{Ni}_3\text{O}_{10}$ [48], which directly implicates phonons. Taken together, these observations suggest that

electron-phonon coupling may play a significant—possibly indispensable—role in stabilizing the DW order, and may also contribute superconductivity once the DW order is suppressed.

In summary, ultrafast optical spectroscopy of $\text{La}_4\text{Ni}_3\text{O}_{10}$ reveals the opening of a strong-coupling density-wave gap, anomalous renormalization of a lattice mode that directly tracks the order parameter, and nonthermal optical melting of the ordered state. The contrasting behavior of phonon modes highlights the selective, multi-orbital nature of electron-phonon coupling in this material. These findings establish the DW in $\text{La}_4\text{Ni}_3\text{O}_{10}$ as a lattice-entangled instability and demonstrate that ultrafast optical excitation provides a powerful, non-equilibrium pathway to manipulate competing orders in nickelates.

This work was supported by the National Natural Science Foundation of China (Grant No. 92265101), the National Key Research and Development Program of China (Grant No. 2022YFA1604204), the Open Project of Beijing National Laboratory for Condensed Matter Physics (Grant No. 2024BNLCMPKF001), the Science and Technology Innovation Program of Hunan province (2022RC3068). The work at Fudan University was supported by the Key Program of the National Natural Science Foundation of China (Grant No. 12234006), the National Key Research and Development Program of China (Grant No. 2022YFA1403202), Quantum Science and Technology-National Science and Technology Major Project (Grant No. 2024ZD0300103), the Shanghai Municipal Science and Technology Major Project (Grant No. 2019SHZDZX01), and the Large Scientific Facility Open Subject of Songshan Lake Laboratory (Grant No. KFKT2022A03).

* These authors contributed equally to this work

† Corresponding author: zhaoj@fudan.edu.cn

‡ Corresponding author: jqmeng@csu.edu.cn

[1] H. Sun, M. Huo, X. Hu, J. Li, Z. Liu, Y. Han, L. Tang, Z. Mao, P. Yang, B. Wang *et al.*, *Nature* **621**, 493 (2023).

[2] Y. Zhu, D. Peng, E. Zhang, B. Pan, X. Chen, L. Chen, H. Ren, F. Liu, Y. Hao, N. Li *et al.*, *Nature* **631**, 531 (2024).

[3] J. Hou, P. T. Yang, Z. Y. Liu, J. Y. Li, P. F. Shan, L. Ma, G. Wang, N. N. Wang, H. Z. Guo, J.-P. Sun *et al.*, *Chin. Phys. Lett.* **40**, 117302 (2023).

[4] Y. Zhang, D. Su, Y. Huang, Z. Shan, H. Sun, M. Huo, K. Ye, J. Zhang, Z. Yang, Y. Xu *et al.*, *Nat. Phys.* **20**, 1269 (2024).

[5] N. Wang, G. Wang, X. Shen, J. Hou, J. Luo, X. Ma, H. Yang, L. Shi, J. Dou, J. Feng *et al.*, *Nature* **634**, 579 (2024).

[6] Q. Li, Y. J. Zhang, Z. N. Xiang, Y. Zhang, X. Zhu, and H. H. Wen, *Chin. Phys. Lett.* **41**, 017401 (2024).

[7] M. Zhang, C. Pei, D. Peng, X. Du, W. Hu, Y. Cao, Q. Wang, J. Wu, Y. Li, H. Liu *et al.*, *Phys. Rev. X* **15**, 021005 (2025).

[8] J. Li, C. Q. Chen, C. Huang, Y. Han, M. Huo, X. Huang, P. Ma, Z. Qiu, J. Chen, X. Hu *et al.*, *Sci. China-Phys. Mech. Astron.* **67**, 117403 (2024).

[9] B. Keimer, S. A. Kivelson, M. R. Norman, S. Uchida, and J. Zaanen, *Nature* **518**, 179 (2015).

[10] Pengcheng Dai, *Rev. Mod. Phys.* **87**, 855 (2015).

[11] M. Shi, Y. Li, Y. Wang, D. Peng, S. Yang, H. Li, K. Fan, K. Jiang, J. He, Q. Zeng *et al.*, *Nat. Commun.* **16**, 2887 (2025).

[12] X. Chen, J. Choi, Z. Jiang, J. Mei, K. Jiang, J. Li, S. Agrestini, M. Garcia-Fernandez, H. Sun, X. Huang *et al.*, *Nat. commun.* **15**, 9597 (2024).

[13] K. Chen, X. Liu, J. Jiao, M. Zou, C. Jiang, X. Li, Y. Luo, Q. Wu, N. Zhang, Y. Guo *et al.*, *Phys. Rev. Lett.* **132**, 256503 (2024).

[14] R. Khasanov, T. J. Hicken, D. J. Gawryluk, V. Sazgari, I. Plokhikh, L. P. Sorel, M. Bartkowiak, S. Botzel, F. Lechermann, I. M. Eremin *et al.*, *Nat. Phys.* **1**, 430 (2025).

[15] D. Zhao, Y. Zhou, M. Huo, Y. Wang, L. Nie, Y. Yang, J. Ying, M. Wang, T. Wu, and X. Chen, *Sci. Bull.* **70**, 1239 (2025).

[16] Z. Liu, H. Sun, M. Huo, X. Ma, Y. Ji, E. Yi, L. Li, H. Liu, J. Yu, Z. Zhang *et al.*, *Sci. China-Phys. Mech. Astron.* **66**, 217411 (2023).

[17] J. Zhang, D. Phelan, A. Botana, Y.-S. Chen, H. Zheng, M. Krogstad, S. G. Wang, Y. Qiu, J. Rodriguez-Rivera, R. Osborn *et al.*, *Nat. Commun.* **11**, 6003 (2020).

[18] M. Kakoi, T. Oi, Y. Ohshita, M. Yashima, K. Kuroki, T. Kato, H. Takahashi, S. Ishiwata, Y. Adachi, N. Hatada *et al.*, *Phys. Soc. Jpn.* **93**, 053702 (2024).

[19] S. Deswal, D. Kumar, D. Rout, S. Singh, and P. Kumar, *arXiv:2411.13933* (2024).

[20] A. Suthar, V. Sundaramurthy, M. Bejas, C. Le, P. Puphal, P. Sosa-Lizama, A. Schulz, J. Nuss, M. Isobe, P. A. van Aken *et al.*, *arXiv:2508.06440* (2025).

[21] M. Li, J. Gong, Y. Zhu, Z. Chen, J. Zhang, E. Zhang, Y. Li, R. Yin, S. Wang, J. Zhao *et al.*, *Phys. Rev. B* **112**, 045132 (2025).

[22] X. Du, Y. Li, Y. Cao, C. Pei, M. Zhang, W. Zhao, K. Zhai, R. Xu, Z. Liu, Z. Li *et al.*, *arXiv:2405.19853* (2024).

[23] Y. Zhang, L. F. Lin, A. Moreo, T. A. Maier, and E. Dagotto, *Phys. Rev. Lett.* **133**, 136001 (2024).

[24] S. Xu, C. Q. Chen, M. Huo, D. Hu, H. Wang, Q. Wu, R. Li, D. Wu, M. Wang, D. X. Yao *et al.*, *Phys. Rev. B* **111**, 075140 (2025).

[25] S. Xu, H. Wang, M. Huo, D. Hu, Q. Wu, L. Yue, D. Wu, M. Wang, T. Dong, and N. Wang, *Nat. Commun.* **16**, 7039 (2025).

[26] H. Li, X. Zhou, T. Nummy, J. Zhang, V. Pardo, W. E. Pickett, J. F. Mitchell, and D. S. Dessau, *Nat. Commun.* **8**, 704 (2017).

[27] Y. Li, Y. Cao, L. Liu, P. Peng, H. Lin, C. Pei, M. Zhang, H. Wu, X. Du, W. Zhao *et al.*, *Sci. Bull.* **70**, 180 (2025).

[28] Q. Y. Wu, C. Zhang, B. Z. Li, H. Liu, J. J. Song, B. Chen, H. Y. Liu, Y. X. Duan, J. He, J. Liu *et al.*, *Phys. Rev. B* **111**, L081110 (2025).

[29] Z. Wang, Q. Wu, Q. Yin, C. Gong, Z. Tu, T. Lin, Q. Liu, L. Shi, S. Zhang, D. Wu *et al.*, *Phys. Rev. B* **104**, 165110 (2021).

[30] Y. Z. Zhao, Q. Y. Wu, C. Zhang, B. Chen, W. Xia, J. J. Song, Y. H. Yuan, H. Liu, F. Y. Wu, X. Q. Ye *et al.*, *Phys. Rev. B* **108**, 075115 (2023).

[31] C. Zhang, Q. Y. Wu, W. S. Hong, H. Liu, S. X. Zhu, J. J. Song, Y. Z. Zhao, F. Y. Wu, Z. T. Liu, S. Y. Liu *et al.*, *Sci. China-Phys. Mech. Astron.* **65**, 237411 (2022).

[32] See the Supplemental Material for additional data of $\text{La}_4\text{Ni}_3\text{O}_{10}$, which include references [33–36].

[33] A. Rothwarf and B. Taylor, *Phys. Rev. Lett.* **19**, 27 (1967).

[34] V. Kabanov, J. Demsar, B. Podobnik, and D. Mihailovic, *Phys. Rev. B* **59**, 1497 (1999).

[35] J. Demsar, J. L. Sarrao, A. J. Taylor, *J. Phys.: Condens. Matter* **18**, R281-R314 (2006).

[36] D. Rout, S. R. Mudi, M. Hoffmann, S. Spachmann, R. Klingeler, S. Singh, *Phys. Rev. B* **102**, 195144 (2020).

[37] Q. Y. Wu, D. Y. Hu, C. Zhang, M. W. Huo, H. Liu, B. Chen, Y. Zhou, Z. T. Fu *et al.*, *Phys. Rev. B* **112**, 235110 (2025).

[38] M. Balkanski, R. Wallis, and E. Haro, *Phys. Rev. B* **28**, 1928 (1983).

[39] J. Menendez and M. Cardona, *Phys. Rev. B* **29**, 2051 (1984).

[40] J. Hasainen, Y. Wu, M. Shi, Y. Zhai, Q. Wu, Z. Liu, Y. Zhou, X. Chen, and J. Zhao, *Proc. Natl. Acad. Sci. USA* **122**, e2406464122 (2025).

[41] B. Loret, N. Auvray, Y. Gallais, M. Cazayous, A. Forget, D. Colson, M. H. Julien, I. Paul, M. Civelli, A. Sacuto, *Nature Physics* **15**, 771 (2019).

[42] D. Oh, D. Song, Y. Kim, S. Miyasaka, S. Tajima, J. M. Bok, Y. Bang, S. R. Park, and C. Kim, *Phys. Rev. Lett.* **127**, 277001 (2021).

[43] H. Y. Huang, A. Singh, C. Y. Mou, S. Johnston, A. F. Kemper, J. van den Brink *et al.*, *Phys. Rev. X* **11**, 041038 (2021).

[44] X. Tang, S. Zhu, H. Liu, C. Zhang, Q. Wu, Z. Liu, J. Song, X. Guo, Y. Wang, H. Ma *et al.*, *Chin. Phys. B* **31**, 037103 (2022).

[45] S. Duan, Y. Cheng, W. Xia, Y. Yang, C. Xu, F. Qi, C. Huang, T. Tang, Y. Guo, W. Luo, *et al.*, *Nature* **595**, 239 (2021).

[46] H. Liu, C. Zhang, Q. Wu, Y. Jin, Z. Zhu, J. Song, S. Cui, Z. Sun, H. Wang, B. Chen *et al.*, *Phys. Rev. B* **111**, L121113 (2025).

[47] Y. Meng, Y. Yang, H. Sun, S. Zhang, J. Luo, L. Chen, X. Ma, M. Wang, F. Hong, X. Wang *et al.*, *Nat. Commun.* **15**, 10408 (2024).

[48] R. Khasanov, T. Hicken, I. Plokhikh, V. Sazgari, L. Keller *et al.*, *arXiv:2503.04400* (2025).